Biosensors and Bioelectronics 50 (2013) 143–149

Contents lists available at SciVerse ScienceDirect

Biosensors and Bioelectronics

journal homepage: www.elsevier.com/locate/bios

# Electrochemical impedance immunosensor based on gold nanoparticles–protein G for the detection of cancer marker epidermal growth factor receptor in human plasma and brain tissue

Reda Elshafey [a], Ana C. Tavares [a], Mohamed Siaj [b], Mohammed Zourob [c,*]

[a] INRS Énergie, Matériaux et Télécommunications, Varennes, Québec, Canada J3X 1S2
[b] Département de Chimie, Université du Québec à Montréal, Case Postale 8888, Succursale Centre-ville, Montréal, Québec, Canada H3C 3P8
[c] Cranfield Health, Cranfield University, Cranfield, Bedfordshire MK43 0AL, UK

ARTICLE INFO

*Article history:*
Received 4 April 2013
Received in revised form
28 May 2013
Accepted 29 May 2013
Available online 18 June 2013

*Keywords:*
EGFR
Cancer biomarker
Protein G
Label-free biosensor
Gold nanoparticles
Plasma

ABSTRACT

A sensitive label-free impedimetric immunosensor for the detection of cancer biomarker epidermal growth factor receptor (EGFR) was developed with a limit of detection as low as 0.34 pg $mL^{-1}$ in PBS and 0.88 pg $mL^{-1}$ in human plasma. The gold nanoparticles were electrodeposited to modify the gold surface and to increase the electrochemical active area by a factor of approximately 3, i.e. by 68%. Protein G was used as scaffold for well oriented EGFR antibodies immobilization. Under optimal experimental parameters, the impedance changes were used for the detection of EGFR with a wide dynamic range of 1 pg $mL^{-1}$–1 μg $mL^{-1}$. The immunosensor showed an excellent reproducibility and selectivity against biomarkers, murine double minute 2 and platelet derived growth factor receptor. The excellent analytical performance of the EGFR immunosensor in terms of selectivity, sensitivity and low detection limit might be attributed to the synergetic effect between the Au nanoparticles and the protein G scaffold. The matrix effect from mouse brain tissue homogenate was also studied and the immunosensor showed excellent recoveries ranging from 98.3% to 115% and RSD of 1.55–6.17. Finally, our developed strategy could open new avenues for clinical screening and prognosis of tumors.



## 1. Introduction

Epidermal growth factor receptor (EGFR, ErbB-1; HER1 in humans) is a cell trans-membrane glycoprotein located at the cell surface. Upon binding with its ligands such as epidermal growth factor (EGF) and transforming growth factor (TGFα), the tyrosine kinase in its intracellular domain activates and induces cell differentiation and proliferation (Bethune et al., 2010). EGFR is over-expressed in many tumors of epithelial origin, such as non-small cell lung cancer (NSCLC), breast, head and neck, gastric, colorectal, esophageal, prostate, bladder, renal, pancreatic, and ovarian cancers (Salomon et al., 1995). Moreover, it is associated with advanced tumor stages, and resistance to standard therapies (chemotherapy and radiation; Sartor, 2000; Chen et al., 2000). Therefore, EGFR could be used as a rational target for antitumor strategies, or as a target for gene therapy.

EGFR has been used as a prognostic marker for many tumors, as its overexpression was correlated to a poor prognosis in breast, gliomas, squamous carcinoma and laryngeal cancers (Arteaga, 2002; Nicholson et al., 2001). In addition, it has been identified as a strong prognostic indicator for aggressive disease stages in head and neck, ovarian, cervical, bladder, and esophageal cancers (Arteaga, 2002). Hence, the development of different methodologies for the quantification of this receptor is highly desired for cancer screening and effective prognosis.

A number of techniques have been employed to detect EGFR. Immunohistochemistry (IHC) is commonly used for the analysis of clinical tumor tissue samples (Sarkis et al., 2010; Hirsch et al., 2008), though it is semi-quantitative. Western blotting (WB) analysis on membranes of cell lyses (Thariat et al., 2012) and Enzyme-linked immunosorbant assay (ELISA) have been also used to estimate the EGFR level (Pfeiffer et al., 1996). However, these techniques are time consuming; require multi-steps and chromophores/fluorophores, or enzymatic tagging. Moreover, IHC and WB techniques require highly qualified labor to conduct the experiments. Therefore, there has been growing interest to develop label-free, time-efficient, and quantitative biosensing-based tools.

Several biosensing platforms have been developed for the detection of the EGFR protein, including a microfluidic based nano-biochip (Weigum et al., 2010), cell-based sensor using lab-on-a-chip (LOC; Weigum et al., 2007), surface plasmon resonance based on gold nanoparticles (El-Sayed et al., 2005), quartz crystal

* Corresponding author. Tel.: +44 1234 758318.
*E-mail address:* m.zourob@cranfield.ac.uk (M. Zourob).

0956-5663/$ - see front matter © 2013 Elsevier B.V. All rights reserved.
http://dx.doi.org/10.1016/j.bios.2013.05.063

microbalance immunosensors (Chen et al., 2011) and zinc oxide thin film transistor-based immunosensor (ZnO-bioTFT; Reyes et al., 2011). Recently, label-free electrochemical immunosensor employing cyclic voltammetry technique for the detection of EGFR with detection limit of 1 pg $mL^{-1}$ was reported (Vasudev et al., 2013). However, the reported EGFR biosensors have limited applications because of many challenges of narrow dynamic range, lower sensitivity, and especially, complicated experimental setup and the cost of apparatus.

Electrochemical impedance spectroscopy (EIS) has become a powerful and informative tool for evaluating the interfacial properties of biochemical and biophysical processes (Barsoukov and Macdonald, 2005). Unlike voltammetric techniques, EIS is non-destructive to the biological interactions because it works under very small amplitude perturbation from steady state. It is also considered a label free technique as it does not require special tagging or reagents (Daniels and Pourmand, 2007). EIS has been employed for biosensors characterization and binding events occurring at modified electrode surfaces, such as, antigen–antibodies (Elshafey et al., 2013; Bryan et al., 2013), DNA hybridization (Xu et al., 2012), and recently for small molecules sensing (Bacher et al., 2012) by monitoring the variation of charge transfer impedance. EIS has been widely employed for many applications (Siddiqui et al., 2012; Xu et al., 2013; Guo et al., 2012) due to its sensitivity and specificity (Mantzila et al., 2008).

Gold nanoparticles (AuNPs) are one of the most promising nanomaterials that opened new horizons for fabrication of novel electrochemical biosensors. AuNPs possess unique properties, including easy preparation, good biocompatibility, excellent conductivity, and large surface area (Ding et al., 2004; Li et al., 2011). Moreover, gold nanoparticle-modified electrodes showed almost 3-fold increase in the electroactive area, leading to increase in functional density of biomolecules and facilitate electron exchange (Liu et al., 2007). So, it is expected that electrochemical immunosensors based on Au nanoparticles will be quite effective as an analytical tool.

Antibody binding proteins such as protein A and protein G are commonly used to immobilize oriented antibodies (Boyle and Reis, 1987). They have the ability to bind non-antigenic (Fc) regions of immunoglobulin G (IgG), leaving the antigen binding sites of the antibody available to bind their target antigens (Gao et al., 2006; Kausaite-Minkstimiene et al., 2010), producing well aligned immobilized antibodies with minimal steric hindrance (Liu et al., 2011). Well-oriented antibodies immobilization increases antigen binding capacity by about 2–8 times and, consequently, lowers the detection limit, improves the sensitivity and increases the immunosensor dynamic range (Turková, 1999).

Herein we report a label-free impedance based immunosensor for the direct assay of EGFR protein. The immunosensor includes Au electrode modified by AuNPs/cysteamine/PDITC/protein G. Gold nanoparticles (AuNPs) were electrochemically deposited on gold surface, followed by cysteamine self-assembled monolayer formation. Next, protein G was attached to the amine-terminated SAMs modified electrodes using 1,4-phenylene diisothiocyanate (PDITC) linker. Then anti-EGFR antibodies bind to protein G modified electrode via their non-antigenic Fc regions. The proposed immunosensor is characterized by employing cyclic voltammetry (CV), square wave voltammetry (SWV) and EIS in the presence of $[Fe(CN)_6]^{3-}$/$[Fe(CN)_6]^{4-}$ redox probe. Before using the immunosensor for testing, a number of key parameters such as concentration of protein G, EGFR antibody, and incubation time of protein G modified electrode with EGFR antibody were optimized. The selectivity of the developed immunosensor was evaluated against other cancer markers platelets derived growth factor receptor (PDGFRα) and murine double minute 2 (MDM2). Finally, the immunosensor was validated for the detection of EGFR in human plasma and mouse brain homogenate tissue.

## 2. Experimental

### 2.1. Chemicals and materials

The list of all reagents employed to fabricate the EGFR is mentioned in Supplementary data.

### 2.2. Assembly of the EGFR immunosensor

Polycrystalline Au electrodes were first polished with alumina slurries of 1.0, 0.3, and 0.05 μm, rinsed with water, sonicated for 5 min and dried with nitrogen; the electrodes were then treated with fresh piranha's solution (1:3, v/v, $H_2O_2$ and $H_2SO_4$) for 5 min and subsequently washed with Milli-Q water, further sonicated in ethanol for 5 min and dried. (*CAUTION*: *piranha solution reacts violently with most organic materials and must be handled with extreme care*). Finally, the Au electrodes were subjected to electrochemical cleaning by scanning the potential between 0.0 and 1.6 V vs. Ag/AgCl(sat.) at 100 mV $s^{-1}$ in 0.1 mol $L^{-1}$ sulfuric acid until the typical voltammetric characteristics of a clean Au electrode were obtained.

Initially, the pre-treated electrodes were dipped into solution of $HAuCl_4 \cdot 3H_2O$ (6 mmol $L^{-1}$) containing 0.1 mol $L^{-1}$ $KNO_3$ as supporting electrolyte (Chen et al., 2011); then the cyclic voltammetry was applied for the electrodeposition of Au nanoparticles using cathodic potential sweep −0.2 to −1.2 V for 20 cycles under nitrogen atmosphere. With this procedure the electrochemical surface area of the gold electrodes was increased by a factor of 3 (see Supporting information for detailed characterization). Self-assembled monolayers of cysteamine were formed by immersing the gold nanoparticle-modified electrodes (AuNPs/Au) in 10 mmol $L^{-1}$ aqueous solution of cysteamine hydrochloride, for 16 h at room temperature, followed by washing the modified electrode with water to remove cysteamine residues and drying. The terminal amino groups of cysteamine modified electrode (Cys/AuNPs/Au) were then activated by immersing the electrodes in 10 mmol $L^{-1}$ PDITC in pyridine and N,N-dimethyl formamide (DMF; v-v, 1:9) for 1 h to form a cross linked monolayer on the SAM modified AuNPs electrode. Then the electrodes were washed several times with DMF and PBS (pH 7.4). The PDITC-modified electrode was incubated in 15 μg $mL^{-1}$ protein G solution in PBS (pH 8.5) for 1 h and rinsed with 0.1% Tween–PBS (pH 8.5) to remove unbound protein G. After that, the protein G-modified electrode was immersed in 0.1 mol $L^{-1}$ of ethanolamine (pH 8.5) for 30 min to deactivate the remaining thiocyanate groups, followed by washing several times with PBS (pH 8.5). Finally, the protein G modified electrodes were dipped in 15 μg $mL^{-1}$ EGFR antibodies solution in PBS (pH 7.4) for 45 min. The EGFR antibody modified electrodes (Ab/PG/PDITC/Cys/AuNPs/Au) are ready to be used for sensing or stored dry at 4 °C for several days without a decrease in the activity. The EGFR immunosensors were incubated for 1 h in standard EGFR antigen or spiked solutions (pH = 7.4) with a concentration varying from 1 pg $mL^{-1}$ to 1 μg $mL^{-1}$, followed by rinsing thoroughly with copious amounts of PBS (pH 7.4) prior to electrochemical measurements. The whole assembling process of the EGFR immunosensor is shown in Fig. 1.

### 2.3. Electrochemical characterization of EGFR immunosensor

The methods and experimental conditions used for the electrochemical characterization of EGFR immunosensor are reported in detail in Supplementary data.

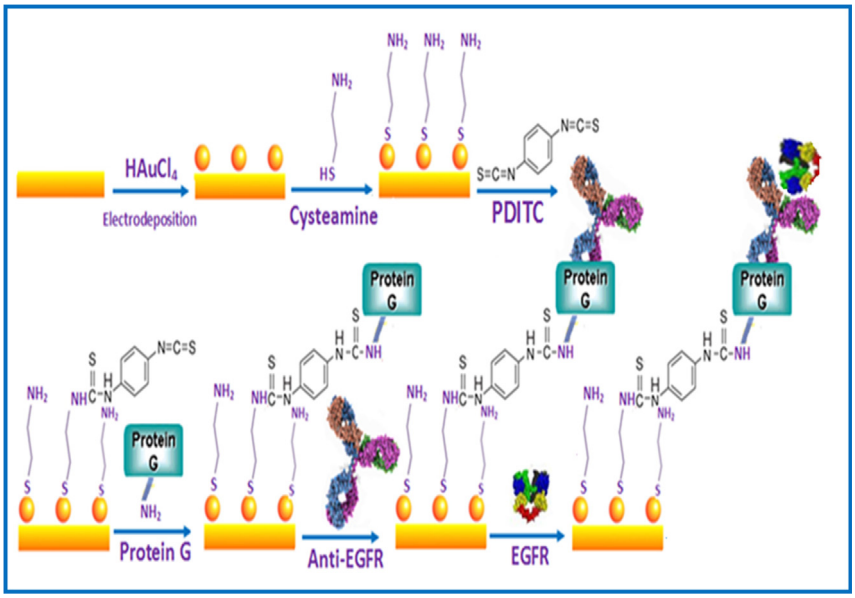


**Fig. 1.** Schematic representation of EGFR immunosensor fabrication on gold electrode.

### 2.4. Real sample analysis

Digestion of mouse brain tissue was performed according to the protocol described in our pervious paper (Elshafey et al., 2013). The detection of EGFR in the tissue homogenate samples was carried out by using EGFR antibody-modified gold electrodes, fabricated as described in Section 2.2. The mouse tissue homogenate and human plasma were freshly diluted with PBS buffer (0.1 M, pH 7.4), followed by spiking of different EGFR concentrations to the range 1 pg $mL^{-1}$–100 ng $mL^{-1}$. The electrodes were then incubated in the diluted samples for 1 h at room temperature, followed by washing with 0.1% Tween–PBS (pH 7.4) solution, before recording EIS signal as described in Section 2.3.

## 3. Results and discussion

### 3.1. Characterization of EGFR immunosensor

CV and SWV have been employed to monitor the fabrication process of the immunosensor using $[Fe(CN)_6]^{3-/4-}$ redox probe. They provide information about the integrity properties of SAM on gold surfaces, such as defects, insulating properties, and the density of the adsorbed layer (Pei et al., 2001; Ding et al., 2005).

Fig. 2(A, B) shows the CVs and the SWVs of $[Fe(CN)_6]^{3-/4-}$ recorded for bare gold electrode Au (a); gold nanoparticles modified electrode (AuNPs/Au) (b); cysteamine-modified gold nanoparticles (Cys/AuNPs/Au) (c); for immobilization of protein G on cysteamine-modified gold nanoparticles using PDITC binding reagent (PG/PDITC/Cys/AuNPs/Au) (d); following the binding of EGFR antibodies to protein G modified electrode (Ab/PG/Cys/PDITC/AuNPs/Au) (e), and finally, after incubation the immunosensor with 100 pg $mL^{-1}$ EGFR antigen standard solution for 1 h (f). Fig. 2A shows a well-defined quasi-reversible redox cyclic voltammogram with an anodic to cathodic peak currents ratio of approximately one and peak-to-peak separation $\Delta E_p$ of 100 mV for the bare gold electrode. After the AuNPs were electrodeposited on the Au electrode surface (Fig. 2A, curve b), the reversibility was kept the same as that for the bare Au electrode, and the peak current ($I_a$=44.2 μA) significantly exceeded that of the bare gold electrode ($I_a$=30.9 μA; Fig. 2A, curve a). Furthermore, the $\Delta E_p$ between the reduction and the oxidation waves decreased to 70.8 mV, suggesting that the electro-deposited AuNPs increased the electrode conductivity and enhanced the electron transfer between the redox probe and electrode surface (Chen et al., 2011). Fig. 2B (curves a, b) shows the same behavior of current change in case of the SWV, but with a slight shift in the anodic peak potential. In case of the cysteamine–AuNPs coated electrodes, Fig. 2A (curve c), the peak current value ($I_a$=43.9 μA) was almost identical to that of the AuNPs modified electrode, but the $\Delta E_p$ between the reduction and the oxidation waves slightly decreased to 68.3 mV. However, as SWV is more sensitive than CV, the peak currents differences were clearly observed for the electrode modification steps (Fig. 2B curves b, c; $I_a$=122.3 μA and $I_a$=139.6 μA, respectively). Moreover, the modification of the AuNPs modified electrodes with cysteamine (Fig. 2B curve c) increased the peak current by 12.4%. This increase is attributed to the electrostatic interaction between the negative charge of $[Fe(CN)_6]^{3-/4-}$ and the terminal positively charged amine moieties of the cysteamine-modified AuNPs coated electrode (Erhan et al., 2011), and might be due to synergetic effect between electro-deposited AuNPs and cysteamine SAM formation.

Indeed, after immobilization of the protein G, the faradaic reaction is highly hindered (accompanied by decrease of both the anodic and cathodic currents and an increase of the peak separation $\Delta E_p$ 92.7 mV) due to the blocking effect of the protein G layer as shown in Fig. 2A (curve d). Fig. 2A (curve e) shows an additional drop in the cathodic and anodic peak currents, and the peak separation $\Delta E_p$ increased to 119.6 mV, upon the binding of the anti-EGFR antibodies to protein G modified electrode via their Fc portions. This might be due to the barrier effect of bulky antibodies molecules as well as their negative charge (isoelectric point 6.1; Yu et al., 2010) in solution of pH 7.4. A further decrease of the peak current and an increase of the peak separation were also observed, after the immunochemical binding of the EGFR antigens (curve f) in Fig. 2A. The same behavior was observed using SWV, Fig. 2B (curves d, e, f). In conclusion, the results of CV and SWV are in agreement with each other and support the success of immunosensor fabrication.

EIS is another informative and commonly used technique to investigate biosensors. It is employed here for the characterization of EGFR immunosensor assembly process in parallel with the cyclic and square wave voltammetry. The impedance spectra represented in the Nyquist plot consist of the semicircle portion

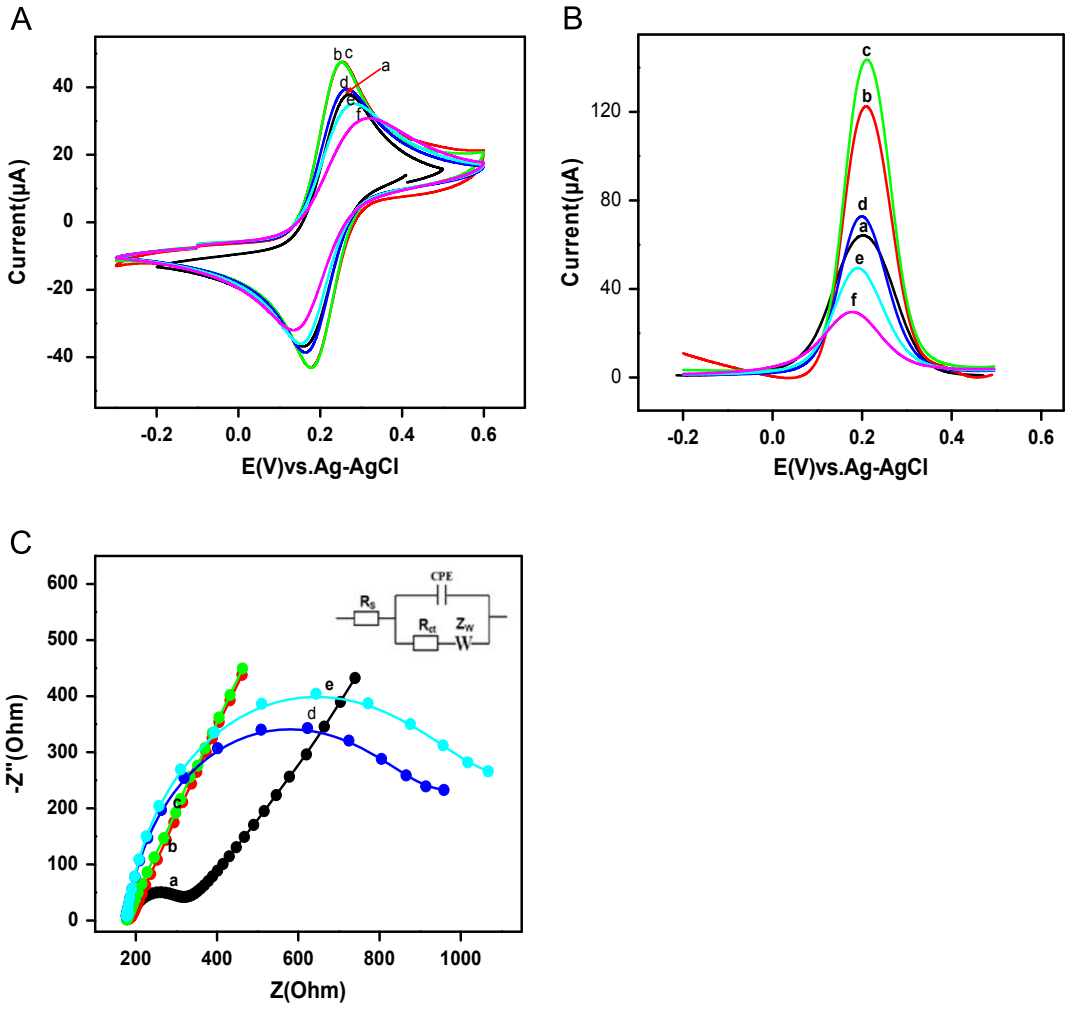


**Fig. 2.** (A, B) CVs and SWVs recorded on bare gold electrodes (a); AuNPs electrodeposition (b); SAM cysteamine modification (c); protein G immobilization (d); antibodies binding to protein G modified electrodes (e); and after immunochemical complex formation between the Ab/PG/PDICT/Cys/AuNPs/Au modified electrode and 100 pg $mL^{-1}$ EGFR solution for 1 h (f), in a 10 mmol $L^{-1}$ PBS, pH 7.4 solution containing 5 mmol $L^{-1}$ $[Fe(CN)_6]^{3-/4-}$ at scan rate of 100 mV $s^{-1}$. (C) Nyquist plots for impedance measurements corresponding to bare gold electrode (a); AuNPs/Au electrode (b); Cys/AuNPs/Au modified electrode (c); PG/PDICT/Cys/AuNPs/Au modified electrode (d); and Ab/PG/PDICT/Cys/AuNPs/Au modified electrode (e) recorded in 5 mmol $L^{-1}$ $[Fe(CN)_6]^{3-/4-}$ probe in PBS, pH 7.4 over the frequency range from $10^5$ to 5 Hz, bias potential +0.21 V and an ac amplitude of 10 mV. The inset is the Randles equivalent circuit used to fit the impedance spectroscopy.

at higher frequencies indicative of an electron transfer process, and the linear part at low frequencies corresponding to the diffusion controlled process.

Modified Randles equivalent circuit (inset Fig. 2C; Tlili et al., 2006) was employed to fit the impedance spectra of the EGFR immunosensor. This circuit consists of the electrolyte resistance between the working and the reference electrode, $R_s$, the Warburg impedance, $Z_W$ associated to the diffusion process of redox probe ions from the bulk solution to the electrode–solution interface, the electron transfer resistance $R_{et}$ and the constant phase element CPE (related to the double layer capacitance).

Table S1 (Supplementary data) reports the values obtained from fitting the experimental data recorded during the immunosensor stepwise fabrication process. As shown the ohmic solution resistance $R_s$ is kept almost constant during the electrode assembly process while $Z_W$ shows a constant value during the protein G and antibody modification steps.

CPE largely depends on the insulating features at the electrode/electrolyte interface, on the surface area of the electrode, and on the thickness of the separation layer. So, CPE values reflect changes that occurred during the electrode elaboration process. The bare Au electrode showed significantly higher CPE value in comparison with the PG/Cys/AuNPs/Au electrode. However, it decreased for antibodies immobilization Ab/PG/Cys/AuNPs/Au, while it increased again upon attachment of EGFR to the sensor surface.

$R_{et}$ controls the kinetics of electron transfer of the redox probe from the solution to the electrode interface. $R_{et}$ shows the largest variation during the assembly process of the immunosensor. Therefore, it is more suitable as a parameter for sensing the interfacial properties of the prepared immunosensor during the fabrication steps.

It is clear from Fig. 2C, and the reported values in Table S1 (Supplementary data), that the bare gold electrode exhibited a very small semicircle at high frequency (curve a) of $R_{et}$ value (223 Ω). When the AuNPs were electrodeposited on the surface of the Au electrode AuNPs/Au (curve b), and cysteamine SAM formation cys/AuNPs/Au (curve c) modified electrodes, the Nyquist plots showed a straight line, as $R_{et}$ turned into zero value, which is a characteristic of a predominantly diffusion limited process (Ensafi et al., 2011). This might be attributed to the combination of high conductivity and large surface area, which efficiently reduced the electron transfer resistance, consequently giving rise to a diffusion controlled process. From previous results of Fig. 2A, B, it is thought that the deposited AuNPs and the positively charged cysteamine monolayer cause an effective electron conduction pathway between the electrode surface and the negative

$[Fe(CN)_6]^{3-/4-}$ probe (Erhan et al., 2011). The immobilization of protein G onto the surface of cys/AuNPs/Au electrodes, Fig. 2C (curve d), enlarged the diameter of the semicircle and $R_{et}$ significantly increased to 603 Ω, due to the blocking of electrode surface by the protein G molecules PG/cys/AuNPs/Au. An additional effective barrier to the electron transfer of $[Fe(CN)_6]^{3-/4-}$ is provided by the bulky antibodies molecules, which might account for the increase in $R_{et}$ value (863 Ω) in case of the binding of EGFR antibodies to protein G modified electrodes Ab/PG/cys/AuNPs/Au. The results obtained from EIS measurements (Fig. 2C) are in good agreement with the results extracted from CV and SWV (Fig. 2A, B), confirming again the successful immobilization of EGFR antibodies on PG modified AuNPs electrodes and fabrication of EGFR immunosensor.

### 3.2. Optimization of key parameters of the immunosensor

Initially, it is necessary to optimize some parameters that could affect the performance of the developed biosensor. The three most important parameters are the concentration of protein G, of anti-EGFR antibody immobilized on the electrode surface, and the incubation time of the protein G modified electrode with the EGFR antibody as shown in detail in Supplementary data. The optimum conditions correspond to 15 μg $mL^{-1}$ of protein G solution, 15 μg $mL^{-1}$ of EGFR solution and 45 min of antibody incubation time. These conditions were used in the subsequent experiments.

### 3.3. Analytical applications of the EGFR immunosensor

Under the optimal assembling conditions, the immunosensor was tested using different standard solutions of EGFR from 1 pg $mL^{-1}$ to 1 μg $mL^{-1}$ at room temperature for 1 h. The immunoreaction between the immunosensor and the analyte was monitored through the variation of the impedance in the presence of $[Fe(CN)_6]^{3-/4-}$ in PBS at pH 7.4 and through the variation of the cathodic peak current of the same probe under the same conditions.

Fig. 3(A, B) shows the impedance spectra and the cyclic voltamogramms for the immunosensor obtained from various EGFR concentrations. As depicted from Fig. 3A, there was a gradual increase of the diameter of the semicircle in the Nyquist plots as the EGFR concentration increased. This indicates a significant increase in the electron transfer resistance and thus increased the barrier for the electron transfer between the redox probe and the electrode surface.

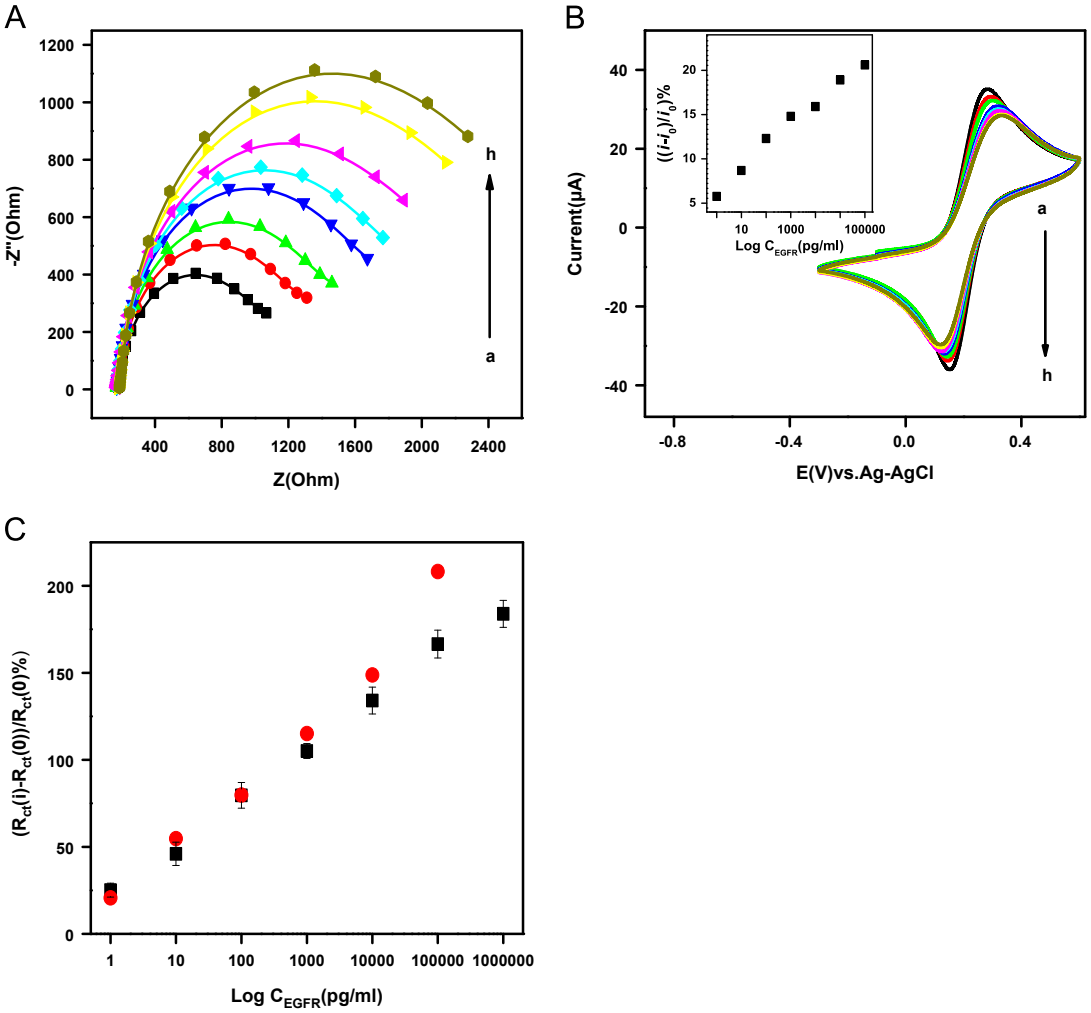


**Fig. 3.** (A, B) Nyquist plots for impedance measurements and cyclic voltammograms of Ab/PG/PDICT/Cys/AuNPs/Au modified electrode at EGFR concentrations of (a) 0 pg $mL^{-1}$ (black), (b) 1 pg $mL^{-1}$ (red), (c)10 pg $mL^{-1}$ (green), (d) 100 pg $mL^{-1}$ (blue), (e) 1 ng $mL^{-1}$ (cyan), (f) 10 ng $mL^{-1}$ (pink), (g) 100 ng $mL^{-1}$ (yellow), and (h) 1 μg $mL^{-1}$ (dark green), in 10 mm $L^{-1}$ PBS in the presence of 5 mm $L^{-1}$ $[Fe(CN)_6]^{3-/4-}$ at pH 7.4. The solid lines correspond to Randles equivalent circuit fits. Inset is the calibration graph corresponding to the increase of $(\Delta i/i_0)$% of the immunosensor with concentration of EGFR. (C) The calibration curve corresponding to the increase of relative electron-transfer resistance $(\Delta R_{et}/R_{et}(0))$% of the immunosensor with concentration of EGFR in human plasma (red) and in PBS (black). Error bars show the standard deviation of three repetitive measurements. (For interpretation of the references to color in this figure legend, the reader is referred to the web version of this article.)

The EGFR immunosensor was developed from different electrodes for reproducibility purpose. The percentage of relative electron transfer resistance values $((R_{et}(i)-R_{et}(0))/R_{et}(0))\%$ was used, and $R_{et}(0)$ and $R_{et}(i)$ are respectively, the electron transfer resistance of the EGFR antibody layer before and after binding with the EGFR antigen. As shown in Fig. 3C (black), there is a linear increase in $(\Delta R_{et}/R_{et}(0))\%$ with increasing concentrations of EGFR from 1 pg mL$^{-1}$ to 1 μg mL$^{-1}$, using the regression equation $(\Delta R_{et}/R_{et}(0))\% = 21.55 + 28.47\log(C)$ pg mL$^{-1}$, $R = 0.996$ $(n = 7)$. To further investigate the reproducibility of the EGFR immunosensor, they were dipped in 10 pg mL$^{-1}$ EGFR standard solution 4 times, and then the impedance responses recorded over 4 times. The immunosensor repeatability was very good with a relative standard deviation of 2.9% for the 10 pg mL$^{-1}$ EGFR concentration. These results showed an acceptable analytical performance of the developed biosensor. The reproducibility of 7 identical biosensors for three repetitive measurements was also examined. The linear detection ranges of these biosensors were found to be between 1 pg mL$^{-1}$ and 1 μg mL$^{-1}$ with relative standard deviation that varied between 4.1% and 6.5%. This indicates that the developed immunosensor has good reproducibility and has a very low limit of detection (LOD), down to 0.34 pg mL$^{-1}$ based on a multiple of 3 × the standard deviation of the baseline signal. Fig. 3B shows also gradual decrease of the reduction peak of $[Fe(CN)_6]^{3-/4-}$ with increasing EGFR concentration, which acts as a barrier for the probe's faradaic current.

Data from cyclic voltammetry was also used to construct a calibration curve (Fig. 3B inset) with regression equation $(\Delta i/i_0)\% = 6.51 + 2.44\log(C)$ pg mL$^{-1}$, $R = 0.991$ $(n = 7)$ and a limit of detection (LOD) down to 0.93 pg mL$^{-1}$ based on a multiple of 3 × the standard deviation of the baseline signal.

Finally, by comparing the LOD calculated from CV and impedance results, a higher sensitivity and accuracy of impedance over the cyclic voltammetry technique is obviously noticed.

Table S2 (see Supplementary information) compares the analytical performance of the EGFR immunosensor with previously reported biosensors. The present work is the first study on the fabrication and testing of impedance based EGFR immunosensor. The developed immunosensor showed superior performance over that of all the other methods in terms of detection limit and dynamic range. This enhanced performance is attributed to the synergistic effect of AuNPs coated electrodes and protein G scaffold. AuNPs increased the electroactive area and subsequently a higher amount of immobilized protein G was achieved. Furthermore, protein G improved the orientation of the immobilized antibodies on the electrode surface thus improving the binding capacity between EGFR and its antibody.

In conclusion, the described protocol based on AuNPs and protein G could be generalized for other cancer markers by changing the specific antibodies for the clinical samples testing with high specificity and sensitivity.

### 3.4. Selectivity of the developed immunosensor

To evaluate the selectivity of the immunosensor, non-specific proteins were used in order to confirm that the change in impedance resulted only from the specific binding of the anti-EGRF modified electrode and its specific antigen. Fig. 4 shows the relative electron-transfer resistance change due to the binding of the non-specific PDGFRα and MDM2 proteins to the EGFR immunosensors. There was an increase of 11.6% and 13.5% in $(\Delta R_{et}/R_0)\%$, when the EGFR modified electrode interacted with 1 ng mL$^{-1}$ PDGFRα and MDM2, respectively, while a 180.5% change was obtained for EGFR. These results confirmed that the recorded impedance changes were induced only by the interaction of the antibody with its EGFR target, and supported the specificity of the immunosensor to EGFR. An additional control experiment using an antibody-free device was also performed at the same EGFR experimental conditions (data not shown). In a third control experiment, an irrelevant anti-MDM2 antibody was used for electrode modification in the same experimental condition as shown in Supplementary data (Fig. S3). No obvious change of the impedance response by the addition of EGFR antigen was found. These results give strong evidence that the proposed immunosensor is highly selective for the detection of EGFR in PBS buffer.

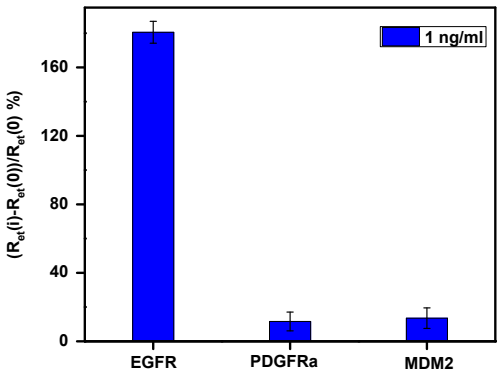


**Fig. 4.** EGFR immunosensor specificity against non-targeted cancer markers PDGFRα and MDM2. The bar graph shows relative electron-transfer resistance $(\Delta R_{et}/R_{et}(0))\%$ of the immunosensor in response to 1 ng mL$^{-1}$ of the cancer markers $(n = 3)$.

### 3.5. Real sample analysis

The potential application of the proposed immunosensor was evaluated by testing it for real sample analysis. Two different matrixes were used, human plasma and mouse brain tissue homogenate. The direct detection of EGFR was performed for spiked EGFR in human plasma and mouse brain tissue homogenate. Fig. 3C (red) presents the calibration plot for the EGFR in human plasma and shows the increase of relative electron-transfer resistance $(\Delta R_{et}/R_{et}(0))\%$ with increasing EGFR concentration. It can be seen that the relative electron-transfer resistance $(\Delta R/R0\%)$ values are linearly proportional to the concentration of EGFR over a wide range of 1 pg mL$^{-1}$–100 ng mL$^{-1}$ in human plasma. The limit of detection was calculated to be 0.88 pg mL$^{-1}$ in human plasma diluted with PBS, based on 3 × the standard deviation of the background signal.

For mouse brain tissue homogenate, we performed spiked and recovery experiments. Initially the mouse brain tissue homogenate was diluted to minimize the matrix effect of biological proteins, followed by spiking of EGFR in concentration range of 10 pg mL$^{-1}$–1 ng mL$^{-1}$. The immunosensors were incubated using the same procedure described above. The recovery results are listed in Table 1, which shows acceptable results with RSD values ranging between 1.55% and 6.17%. The EGFR recoveries are between 98.3% and 115%, which clearly indicate the potentiality of the present EIS-based EGFR immunosensor for EGFR detection in real mouse brain tissue samples.

The analytical performance of the developed immunosensor in diluted normal brain tissue and human plasma are comparable to the performance in PBS, indicating that the detection of the EGFR in these matrixes is also applicable. Therefore, the presented approach may be of potential value for EGFR assay in real biological samples.

**Table 1**
Spike and recovery results ($n=3$) obtained from the EGFR immunosensor in brain mouse homogenate extract.

| EGFR added (pg mL$^{-1}$) | EGFR found (pg mL$^{-1}$) | RSD% | Recovery (%) |
|---|---|---|---|
| 10 | $11.5 \pm 0.71$ | 6.17 | 115 |
| 100 | $101.86 \pm 2.32$ | 2.27 | 110.8 |
| 1000 | $983.33 \pm 15.27$ | 1.55 | 98.3 |

## 4. Conclusions

Here we report a simple and novel electrochemical impedimetric immunosensor for ultrasensitive detection of EGFR using gold nanoparticles and protein G scaffold. The electrodeposition of AuNPs increased the electroactive area by a factor of 3. The utilization of protein G showed well oriented immobilization of EGFR antibodies, as a result of the affinity binding to their Fc portion. The immunosensor showed good reproducibility, excellent sensitivity and could be used as an alternative to the time-consuming conventional approaches. The present immunosensor successfully detected EGFR down to 0.34 pg mL$^{-1}$ in PBS buffer and 0.88 pg mL$^{-1}$ in human plasma. The matrix effect from mouse brain tissue homogenate was also investigated and showed excellent recoveries ranging from 98.3% to 115% and RSD of 1.55–6.17.

## Acknowledgments

The authors would like to extend a special gratitude to the ISS network, NSERC and NanoQuebec for funding. The authors also acknowledge Dr. Andy Ng for his revision and corrections of the manuscript.

## Appendix A. Supporting information

Supplementary data associated with this article can be found in the online version at http://dx.doi.org/10.1016/j.bios.2013.05.063.

## References

Arteaga, C.L., 2002. The Oncologist 7, 31–39.
Bacher, G., Pal, S., Kanungo, L., Bhand, S., 2012. Sensors and Actuators B 168, 223–230.
Barsoukov, E., Macdonald, J.Ross (Eds.), 2005. Impedance Spectroscopy: Theory, Experiment, and Applications, second ed. Wiley Interscience, New Jersey.
Bethune, G., Bethune, D., Ridgway, N., Xu, Z., 2010. Journal of Thoracic Disease 2, 48–51.
Boyle, M.D.P., Reis, K.J., 1987. Nature Biotechnology 5, 697–703.
Bryan, T., Luo, X., Bueno, P.R., Davis, J.J., 2013. Biosensors and Bioelectronics 39, 94–98.
Chen, J-C., Sadhasivam, S., Lin, F-H., 2011. Process Biochemistry 46, 543–550.
Chen, X., Yeung, T.K., Wang, Z., 2000. Biochemical and Biophysical Research Communications 277, 757–763.
Chen, Z., Li, L., Zhao, H., Guo, L., Mu, X., 2011. Talanta 83, 1501–1506.
Daniels, J.S., Pourmand, N., 2007. Electroanalysis 19, 1239–1257.
Ding, S-J., Chang, B-W., Wu, C-C., Lai, M-F., Chang, H-C., 2005. Electrochimica Acta 554, 3–51.
Ding, Y., Chen, M., Erlebacher, J., 2004. Journal of the American Chemical Society 126, 6876–6877.
El-Sayed, I.H., Huang, X., El-Sayed, M.A., 2005. Nano Letters 5, 829–834.
Elshafey, R., Tlili, C., Abulrob, A., Tavares, A.C., Zourob, M., 2013. Biosensors and Bioelectronics 39, 220–225.
Ensafi, A.A., Taei, M., Rahmani, H.R., Khayamian, T., 2011. Electrochimica Acta 56, 8176–8183.
Erhan, D., Ozer, K., Mustafa, K.S., Cagrı, A., Aylin, A, 2011. Biosensors and Bioelectronics 26, 3806–3811.
Gao, D., McBean, N., Schultz, J.S., Yan, Y., Mulchandani, A., Chen, W., 2006. Journal of the American Chemical Society 128, 676–677.
Guo, X., Kulkarni, A., Doepke, A., Halsall, B.H., Iyer, S., Heineman, W.R., 2012. Analytical Chemistry 84, 241–246.
Hirsch, F.R., Dziadziuszko, R., Thatcher, N., Mann, H., Watkins, C., Parums., D.V., Speake, G., Holloway, B., Bunn Jr., P.A., Franklin, W.A., 2008. Cancer 112, 1114–1121.
Kausaite-Minkstimiene, A., Ramanaviciene, A., Kirlyte, J., Ramanavicius, A., 2010. Analytical Chemistry 82, 6401–6408.
Li, F., Feng, Y., Dong, P., Yang, L., Tang, B., 2011. Biosensors and Bioelectronics 26, 1947–1952.
Liu, S., Wang, L., Zhao, F., J, 2007. Electroanalytical Chemistry, 602, 55–60.
Liu, X., Zhao, R., Mao, W., Feng, H., Liu, X., Wong, D.K.Y., 2011. Analyst 136, 5204–5210.
Mantzila, A.G., Maipa, V., Prodromidis, M.I., 2008. Analytical Chemistry 80, 169–1175.
Nicholson, R.I., Gee, J.M.W., Harper, M.E., 2001. European Journal of Cancer 37, S9–S15.
Pei, R., Cheng, Z., Wang, E., Yang, X., 2001. Biosensors and Bioelectronics 16, 355–361.
Pfeiffer, P., Nexo., E., Bentzen, SM., Clausen, PP., Andersen, K., Rose, C., 1996. British Journal of Cancer 78, 96–99.
Reyes, P.I., Ku, C-J., Duan, Z., Lu, Y., Solanki, A., Lee, K-B., 2011. Applied Physics Letters 98, 173702–173704.
Salomon, D.S., Brandt, R., Ciardiello, F., Normanno, N., 1995. Critical Reviews in Oncology/Hematology 19, 183–232.
Sarkis, S.A., Abdullah, B.H., Abdul Majeed, B.A., Talabani, N.G., 2010. Head and Neck Oncology 2, 13–20.
Sartor, C.I., 2000. Seminars in Oncology 27, 15–20.
Siddiqui, S., Dai, Z., Stavis, C.J., Zeng, H., Moldovan, N., Hamers, R.J., Carlisle, J.A., Arumugam, P.U., 2012. Biosensors and Bioelectronics 35, 284–290.
Thariat, J., Etienne-Grimaldi, M-C., Grall, D., Bensadoun, R-J., Cayre, A., Penault-Llorca, F., Veracini, L., Francoual, M., Formento, J-L., Dassonville, O., De Raucourt, D., Geoffrois, L., Giraud, P., Racadot, S., Morinière, S., Milano, G., Obberghen-Schilling, E.V., 2012. Clinical Cancer Research 18 (5), 1313–1322.
Tlili, A., Abdelghani, A., Ameur, S., Jaffrezic-Renault, N., 2006. Materials Science and Engineering C 26, 546–550.
Turková, J., 1999. Journal of Chromatography B: Biomedical Sciences and Applications 722, 11–31.
Vasudev, A., Kaushik, A., Bhansali, S., 2013. Biosensors and Bioelectronics 39, 300–305.
Weigum, S.E., Floriano, P.N., Christodoulides, N., McDevitt, J.T., 2007. Lab on a Chip 7, 995–1003.
Weigum, S.E., Floriano, P.N., Redding, S.W., Yeh, C-K., Westbrook, S.D., McGuff, Stan, Lin, H, Miller, A., Villarreal, F.R., Rowan, F., Vigneswaran, S.D., Williams, N., McDevitt, J.T., M.D., 2010. Cancer Prevention Research 3, 518–528.
Xu, H., Wang, L., Ye, H., Yu, L., Zhu, X., Lin, Z., Wu, G., Li, X., Liu, X., Chen, G., 2012. Chemical Communications 48, 6390–6392.
Xu, M., Luo, X., Davis, J.J., 2013. Biosensors and Bioelectronics 39, 21–25.
Yu, J., Javier, D., Yaseen, M.A., Nitin, N., Richards-Kortum R.,, R, Anvari, B., Wong, M. S., 2010. Journal of the American Chemical Society 132, 1929–1938.